Int. J. Electrochem. Sci., 12 **(2017)** 3483 – 3502, doi: 10.20964/2017.04.105

International Journal of
ELECTROCHEMICAL
SCIENCE
www.electrochemsci.org

Electrochemical Investigations of Simulated Surface Scales Formed on X65 and J55 Pipeline Steel

Rabab M. El-Sherif [1,*], *Giovanna Gabetta* [2]

[1] Chemistry Department, Faculty of Science, Cairo University, 12613 Giza, Egypt
[2] eni e&p Division, San Donato Milanese, Italy
[*]E-mail: rabab1774@yahoo.com

Received: 1 February 2017 / *Accepted:* 27 February 2017 / *Published:* 12 March 2017

Scale formation is considered one of the most important factors that control the rate of corrosion in CO_2 / H_2S containing environments typical of oil and gas plants. To a better understanding of corrosion processes and to implement the existing models, there is a need for the characterization of surface films. This is not an easy task, due to the complexity of the scales themselves, and to the dimension of the layers. In this respect, surface iron carbonate scales formed in service were compared with similar simulated scales obtained in the laboratory. Scale samples were characterized using Scanning Electron Microscopy, Electron Diffraction X-ray (EDX), X-Ray diffraction (XRD), Linear Polarization Resistance (LPR) and Electrochemical Impedance Spectroscopy (EIS). The obtained results demonstrated that the optimized synthetic conditions allow reproducing the field samples at a good level.

Keywords: Corrosion; surface scale; pipeline steel; Impedance; SEM

1. INTRODUCTION

The role of surface films on the corrosion rate has been investigated since a long time to implement models. Scale formation is an important factor governing the rate of corrosion in CO_2 / H_2S containing environments typical of hydrocarbon transportation [1]. The growth of a surface film from outside to inside the metallic wall of the pipe consumes the metal, and in the mean time can restrain the corrosion process by acting as a diffusion barrier for the species involved and by preventing the underlying steel from further dissolution. Electrochemical methods have been broadly used to examine the corrosion layers formed on steel in atmospheric condition. Some authors [1-6] explained the relationships between corrosion and the corrosion layers and asserted that a mass transport limited current plateau is because of the corrosion product layer formation. They declared that the rate of mass

transport of ferrous ions from the layer into the solution is dominating the rate of dissolution at the limiting current. Corrosion products play a crucial role in carbon dioxide corrosion. It has been recommended that the corrosion product layers formed on steel in carbon dioxide environment are composed of an insoluble corrosion product, iron carbonate ($FeCO_3$), and/or undissolved component from the steel, namely cementite (Fe_3C). Two types of corrosion product layers were recognized, one layer is protective, and the other is not [7-15]. The formed protective layer on the steel surface was expected to be porous and the corrosion was inhibited by the diffusion of ions through the layer. All the results above, however, were obtained from a Rotating Cylinder Electrode system (RCE). Little data is accessible concerning the electrochemical characterization of corrosion layers formed on steel in a pipe flow. Field observations do confirm that a pipeline section can be truly harmed, while different parts of a same pipeline, transporting similar liquids, remains practically unattached. Flow regime and flow dynamics-influencing corrosion phenomena-are expected to have a strong effect on the observed behavior of a pipeline and the properties of the surface films. In the attempt of quantifying this contribution, CFD codes were applied to rotating cage specimens with and without obstacles and strains due to fluid, were estimated [1]. More recently, the same tool was allowed to model the shear stress value in a field case where corrosion-erosion was observed [3, 4].

In this work, we aimed at giving a further contribution to this problem. The main objective of the present work is the electrochemical characterization of the surface scales formed during corrosion processes in pipelines transporting multiphase fluid and containing CO_2 and/or H_2S, to implement the corrosion rate predictive models. In this respect, the scale layers on the specimens under controlled/reproducible situations were examined and compared with the field specimens. The morphology, composition and electrochemical behavior of the formed layers were examined.

2. EXPERIMENTAL

2.1. Materials

Table 1. List of the examined samples.

Substrate	Surface film	note
Steel J55 (VETEC J55 sample 1)	Iron Carbonate ($FeCO_3$)	Grown in glass cell (in Laboratory)
Steel J55 (VETEC J55 sample 2)	Iron Carbonate ($FeCO_3$)	Grown in autoclave (in Laboratory)
Steel X65 (VETEC X65 sample 1)	Iron Carbonate ($FeCO_3$)	Grown in glass cell (in Laboratory)
Steel X65 (VETEC X65 sample 2)	Iron Carbonate ($FeCO_3$)	Grown in autoclave (in Laboratory)
Pipeline Ragusa (Multiphase oil pipeline)	Mainly Iron Carbonate ($FeCO_3$)	Grown in field
Pipeline Pakistan (Gas pipeline)	Mainly Iron Carbonate ($FeCO_3$)	Grown in field

Table 2. Chemical compositions of the material samples

Element %	J55	X65
C	0.35	0.048
Si	0.39	0.21
Mn	0.87	1.40
P	0.0015	0.022
S	0.008	0.018
Cr	0.13	-
Ni	0.12	0.20
Mo	0.018	0.01
Cu	0.23	0.04
Nb	-	0.007
Ti	-	0.04
Al	0.007	-
V	-	-

The selected samples for the examination are summarized in Table 1. They were provided by the institute of Venezia Technology, Italy. Two specimens were cut from the field service samples [called, Ragusa and Pakistan] and four samples (VETEC J55, X65 samples 1, 2) were prepared in the laboratory with two different conditions, as will be described in the next section 2.2. Samples are made in Steels X65 (pipeline steel) and J55 (casing steel). The chemical compositions of the steels are presented in Table 2. Specimens are squares 20 x 20 x 3 mm. Substrates were polished up to P600 grade and degreased with acetone.

2.2. Sample scale preparation

Iron carbonate ($FeCO_3$) films were prepared in the laboratory in two conditions characterized by different CO_2 pressure (1bar and 170 bar). In the first case (VETEC J55 sample 1, VETEC X 65 sample 1), the method involved applying to the sample a current equivalent to a forced corrosion rate of 1 mm/year, to get a thick enough layer in a short time. The environment was a solution of NaCl, 1% by weight in a glass reactor. The solution was de-aerated in a flow of CO_2 and heated to 80°C. The pH value was corrected to 6.6 by adding a de-aerated solution of $NaHCO_3$. The corrosion rate was measured with a linear polarization resistance (LPR), and then Fe^{2+} ions were introduced as $FeCl_2$ solution in order to support the rapid growth of the carbonate layer, increasing the over-saturation [3, 4]. After 24 hours the current was removed and the free corrosion rate was measured again. To obtain films in the high pressure of CO_2 and H_2S (VETEC J55 sample 2, VETEC X65 sample 2), an autoclave in Hastelloy C276 was used.

Test conditions to obtain Carbonate films were:

- Fluid: synthetic formation water
- CO_2 pressure: 170 bar
- Temperature: 70°C
- Test duration: 68 hours

Electrochemical and surface tests were done on all the samples.

2.3. Morphological Observations

All the samples were observed with optical and electronic microscopy. X-ray diffraction (XRD) analysis was used to recognize the scale composition. Thickness measurements were performed on SEM micrographics and with a magnetic method (Delta scope MP30E-S). Film characterization (SEM, EDX) was performed using JEOL JXA-840A Electron probe micro-analyzer

2.4. Electrochemical tests

Electrochemical impedance spectroscopy and linear polarization resistance (EIS and LPR) for both the field and the simulated laboratory samples were carried out using the electrochemical workstation IM6e Zahner-Elektrik. The convention three-electrode electrochemical cell with a saturated calomel reference electrode (SCE) and a Platinum auxiliary electrode was used. The amplitude of the superimposed AC-signal was 10 mV peak-to-peaks. The technique included direct estimations of the impedance (Z) and the phase shift (Θ) of the electrochemical system in the frequency range [0.1-10^5 Hz]. The impedance data was investigated using software provided with IM6e Zahner-Elektrik workstation. Linear polarization resistance (LPR) measurements were performed using a scan rate 2 mV/s after 180 minutes of the electrode immersion in the test solution. All experiments have been carried out at room temperature; 25±1°C in 1% NaCl solution. The details of the experimental work are described elsewhere [16, 17].

3. RESULTS AND DISCUSSION

3.1 Morphology of the carbonate film

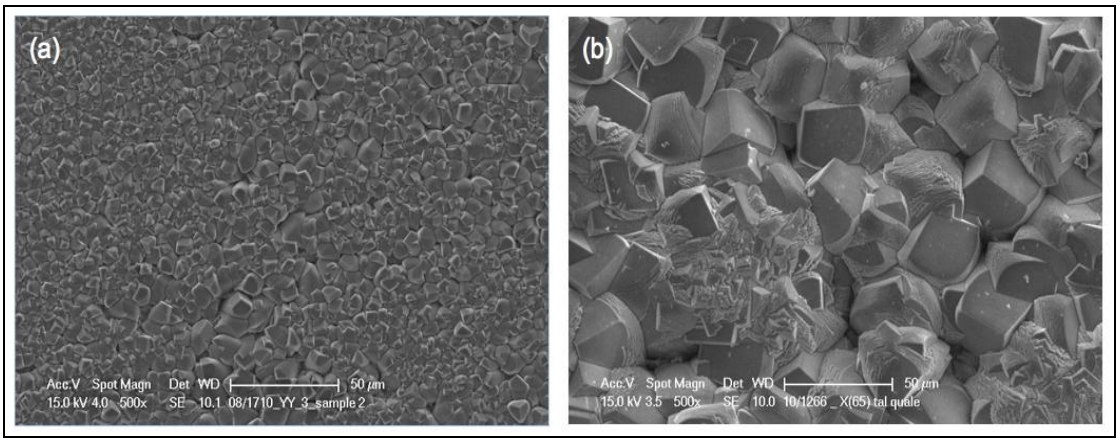

Figure 1. SEM micrographs for the morphology of carbonate scales obtained at two different pressure of CO_2 (a) 1 bar, (b) 170 bar.

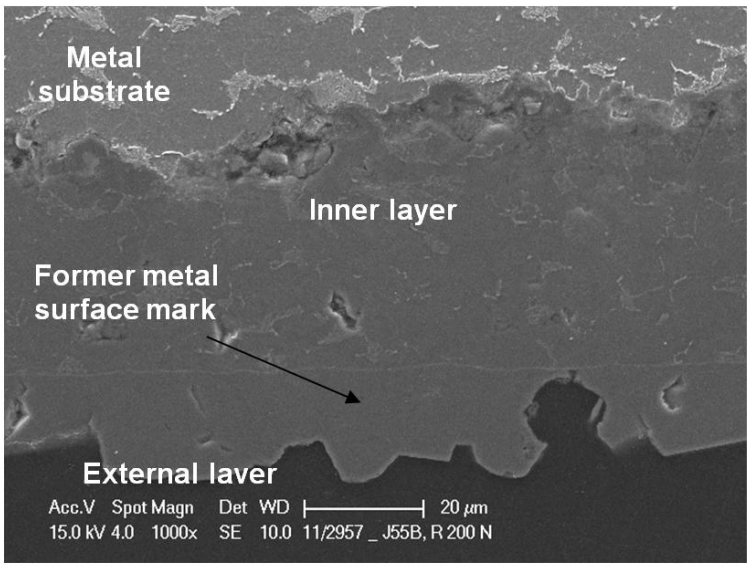

Figure 2. SEM describes the evidence of the two layers in the carbonate formation.

Scanning electron microscopy (SEM) micrographs in Fig. 1 showed the different scales morphology of the two laboratory prepared samples. Crystals obtained in a supercritical CO_2 are larger and the thickness of the film is lower (about 10 μm for films obtained at high pressure, while at 1 bar the film thickness is (40-60 μm) as seen in Fig. 1 (a, b). Fig. 2 described the evidence of the presence of a double layer, as indicated in the literature [4, 5]: at high CO_2 pressure, an internal layer formed was iron carbonate containing Cementite, covered by an outer porous layer formed by large carbonate crystals. The double layer is less evident, or absent, in films formed at low CO_2 pressure. However, steels may have diverse microstructures relying upon the chemical composition and on the manufacture process. Consequently, steels may have different microstructural components (ferrite, perlite, bainite, martensite) which impact their mechanical properties as well as the corrosion resistance of the material [18]. The nature of the base alloy (composition, heat treatment) and the environment (pH, temperature, and CO_2 partial pressure) affects deeply on the protectiveness of the surface film. In our case in a reactor at high CO_2 pressure, it was observed an internal layer where the Perlite phase was converted into Iron carbonate together with the cementite phase not altered by corrosion phenomena and an external layer formed by large Iron carbonate crystals. This conglomerate of crystals did not give rise to a true polycrystal. The double layer was less evident, or absent, in films formed at low CO_2 pressure, as for instance in a glass cell.

3.1.1. Field Specimens

For a pipeline "Ragusa sample" (Multiphase oil pipeline) (Fig. 3 a), it was detected species assignable to a primary corrosion phenomena (observed with the relative frequency signals S, reflecting a joint attack CO_2/H_2S, where the latter could take a minority weight). The distinctive morphological characteristic of the formed corrosion products layers in the massive part of the metal was given by the presence of strings of cementite: however, it was difficult to identify with certainty a

separation surface/interface between the two layers. It was noted that the layers (internal and external) are compacted into a single body, with dividing lines evident only on rare occasions, and presumably the same as the old grain boundaries of the metallic phase**.**

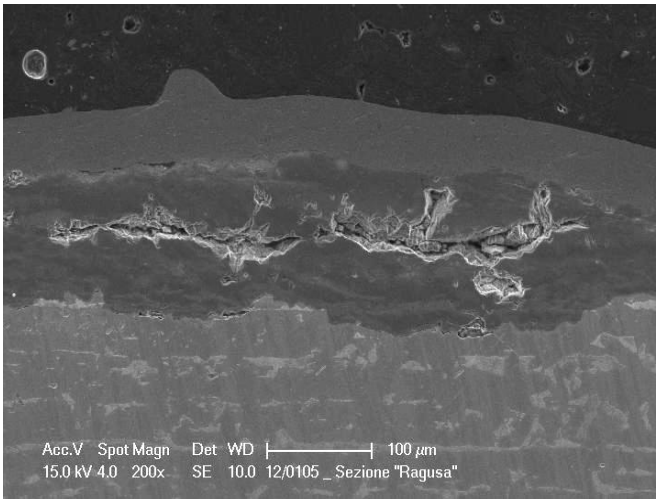

Figure 3. a RAGUSA sample : crater with corrosion products (HE, 200x).

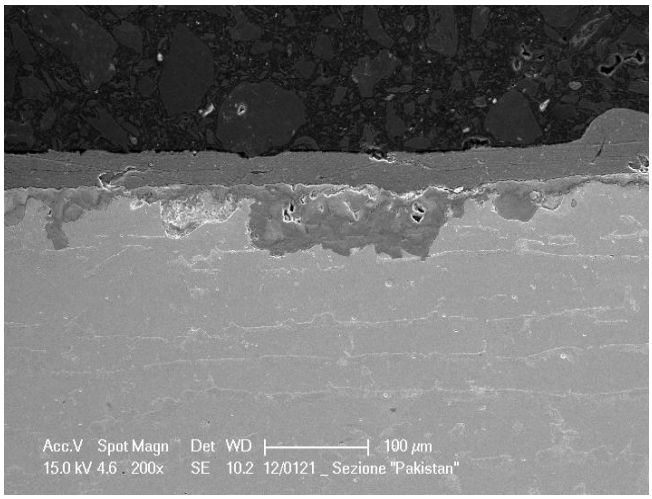

Figure 3. b PAKISTAN sample: not limited vision in the average size of the craters (SE, 200x).

For the pipeline "Pakistan sample" (Gas pipeline) (Fig. 3 b), it was observed craters containing corrosion products, morphologically similar to those of the sample Ragusa craters with corrosion products in a mixed morphology.

3.1.2 Samples prepared in Laboratory

Scanning electron microscopy of the laboratory simulated samples in Fig. 4 a, b allowed the identification of two iron carbonate films with very different morphology. The outer film is less

regular and the inner film maintained a record of a typical original structure of the steel. In the metallurgical structure of the metal substrate, arisen bands through dark areas corresponded to Perlite (area with two phases: Cementite and Ferrite) was observed, whereas the light areas corresponded to grains of the ferrite phase. The corroded substrate showed a geometrically similar structure by dark zones of iron carbonate and light areas of Cementite and iron carbonates. The outer film has a very different morphology with large Iron carbonate crystals (size 20-25 μm) typical of a deposition phenomenon.

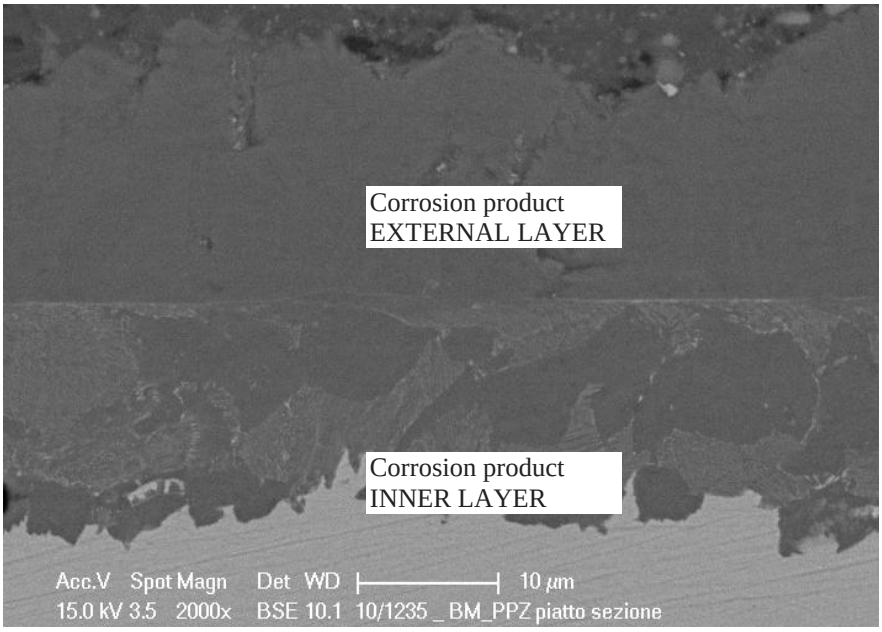

Figure 4. a SEM of J55 steel substrate with iron carbonate layer.

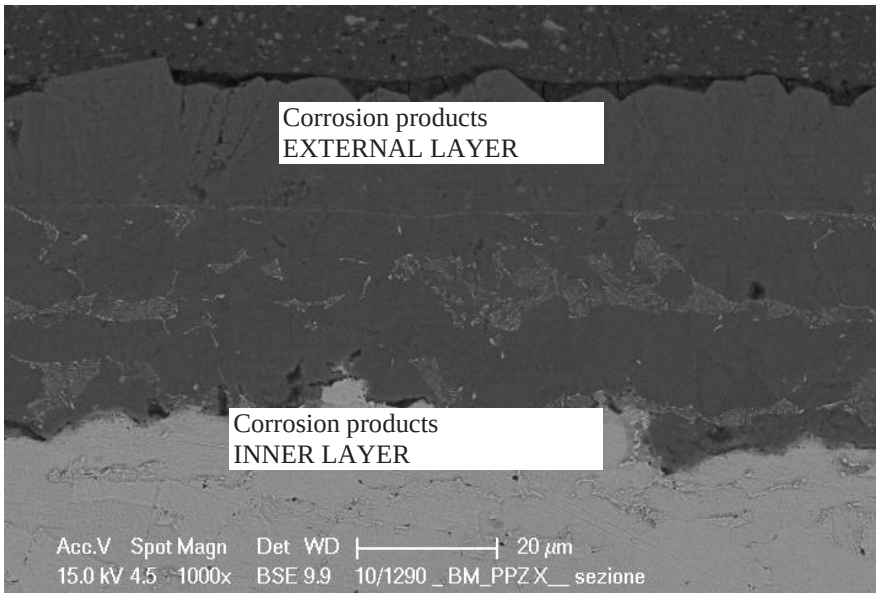

Figure 4. b SEM of X65 steel substrate with iron carbonate layer.

Generally, the expected CO_2 corrosion reactions of carbon steel in anaerobic aqueous solution are [19, 20]:

$$2H_2CO_3 + 2e^- \rightarrow 2H^+ + 2HCO_3^- \quad (1)$$
$$2HCO_3^- + 2e^- \rightarrow 2CO_3^{2-} + 2H^+ \quad (2)$$
$$2H^+ + 2e^- \rightarrow H_2 \quad (3)$$

$$Fe \rightarrow Fe^{2+} + 2e^- \quad (4)$$
$$Fe^{2+} + CO_3^{2-} \rightarrow FeCO_3 \quad (5)$$
$$Fe^{2+} + 2HCO_3^- \rightarrow Fe(HCO_3)_2 \rightarrow FeCO_3 + CO_2 + H_2O \quad (6)$$

The corrosion products such as $FeCO_3$ and $Fe(HCO_3)_2$ are formed with time, and partially passivate the steel surface due to their limited solubility. Hausler, Stegmann [21] and Dugstad [22] suggested that the corrosion films affect significantly on the corrosion rate of carbon steel. This may also, influences the efficiency of the corrosion control by altering the chemical nature of the steel surface.

3.2. Thickness measurements and EDX analysis

Thickness measurements of the scales were made on micrographics. Results obtained on carbonate scales were summarized in Table 3.

Table 3. Thickness of carbonate scales.

Substrate	Environment	Film	Micrographics Thickness (μm)
X65	170 bar CO_2	External	15-20
		Internal	40
J55	170 bar CO_2	External	20
		Internal	15-20

First of all, different films could be formed on the components materials, with different thicknesses and properties. Laboratory tests need to be carefully controlled to obtain reproducible layers, and the obtained layers shall be compared with films grown under service conditions. Of course, the exposition to Oxygen, air and/or environments different from the original one are of importance for the evolution of the film. The methods to grow surface films developed in the frame of the present work seemed to be able to give reproducible and representative layers on the pipeline steel. XRD analysis (Fig. 5) showed that Iron Carbonate was presented as Siderite in both types of samples.

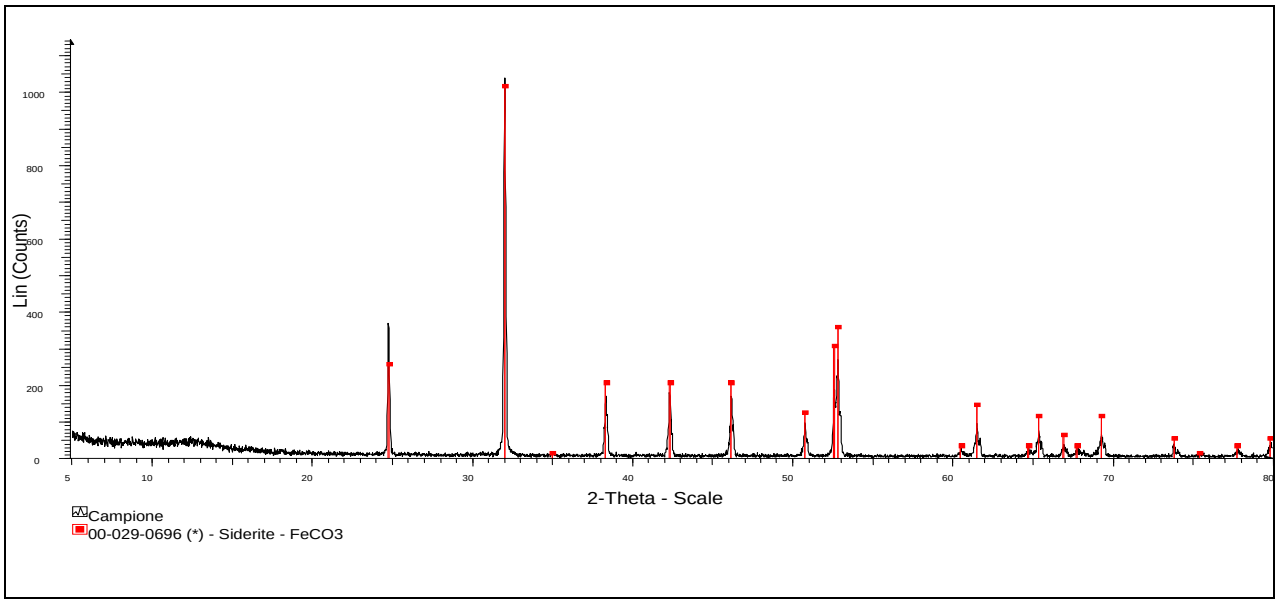

Figure 5. XRD spectrum of the Carbonate layer.

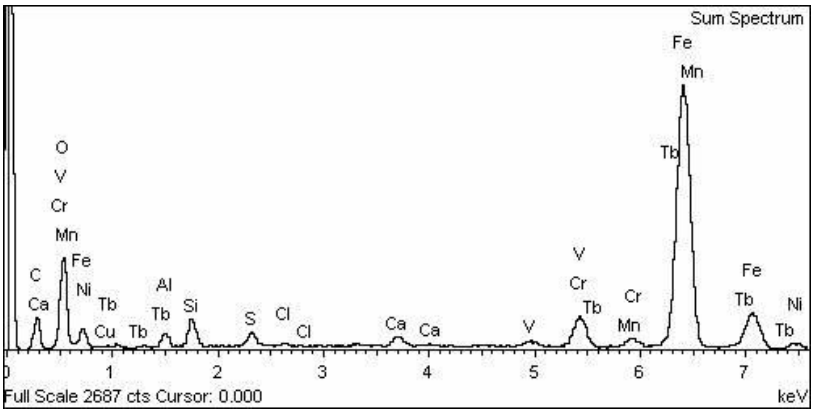

Figure 6. a EDX of a service sample (Pakistan).

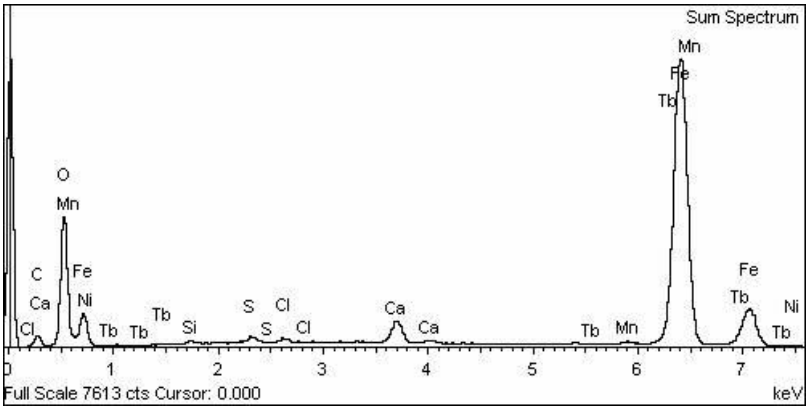

Figure 6. b EDX of a service sample (Ragusa).

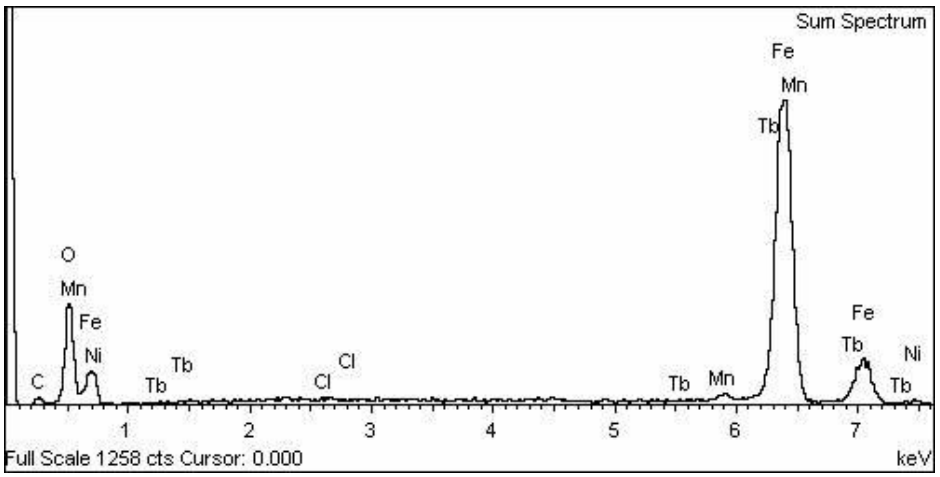

Figure 6. c EDX of Lab-sample [VETEC X65 Sample (1)].

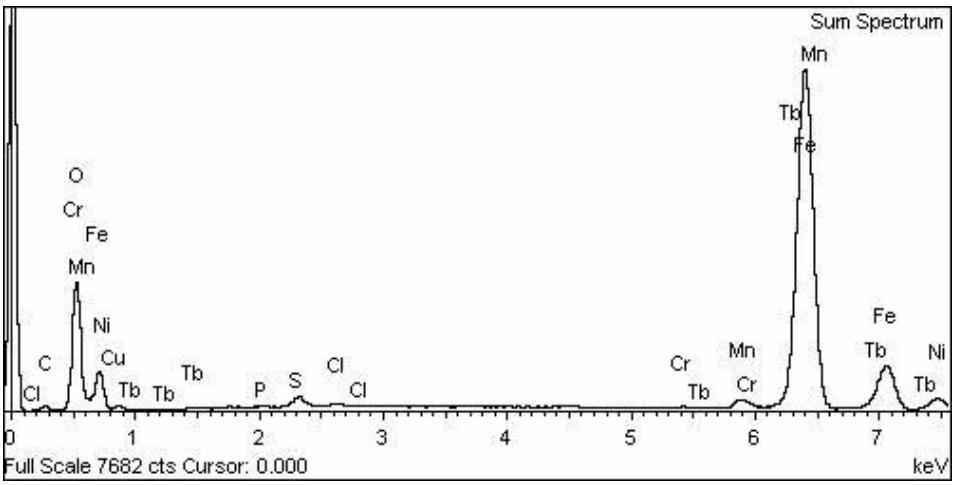

Figure 6. d EDX of Lab-sample [VETEC J55 Sample (1)].

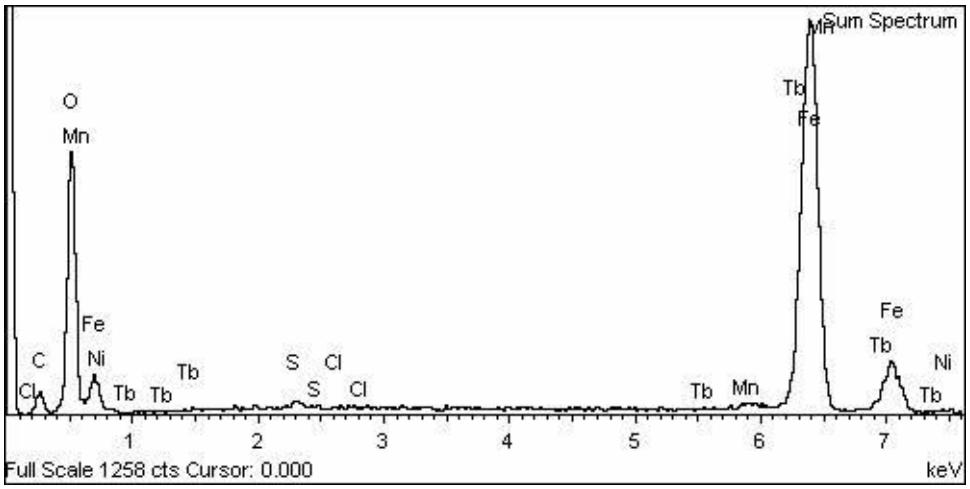

Figure 6. e EDX of Lab-sample [VETEC X65 Sample (2)].

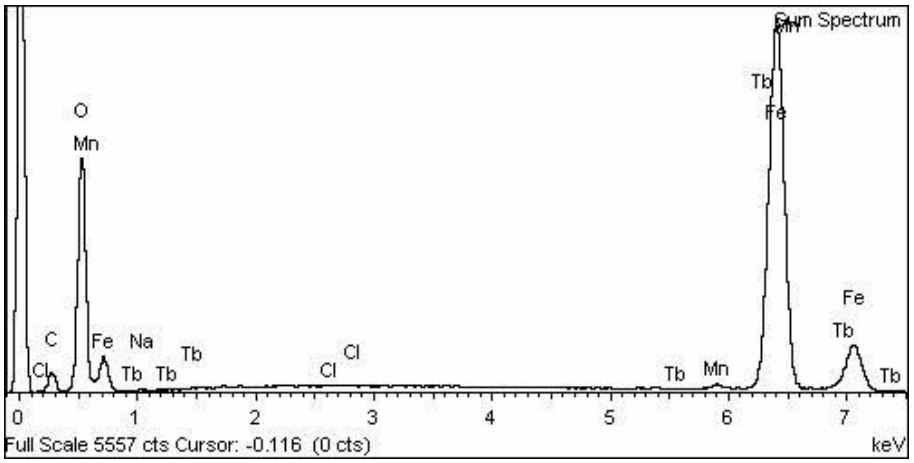

Figure 6. f EDX of Lab-sample [VETEC J55 Sample (2)]**.**

The elemental analysis shown in Fig. 6 (a-f) did not provide discriminating information. The stoichiometry of the compounds presented in the layered deposits was not clearly defined: it was noted, however, a weak but clear change in the contents of "C" and "O" compared with cords of corrosion products/scales, side by side, or above.

3.3 Electrochemical Impedance Spectroscopy and Linear Polarization measurements

Electrochemical impedance spectroscopy (EIS) is considered as a valuable technique for studying the corrosion product scales and their mechanisms of formation and protection [23].

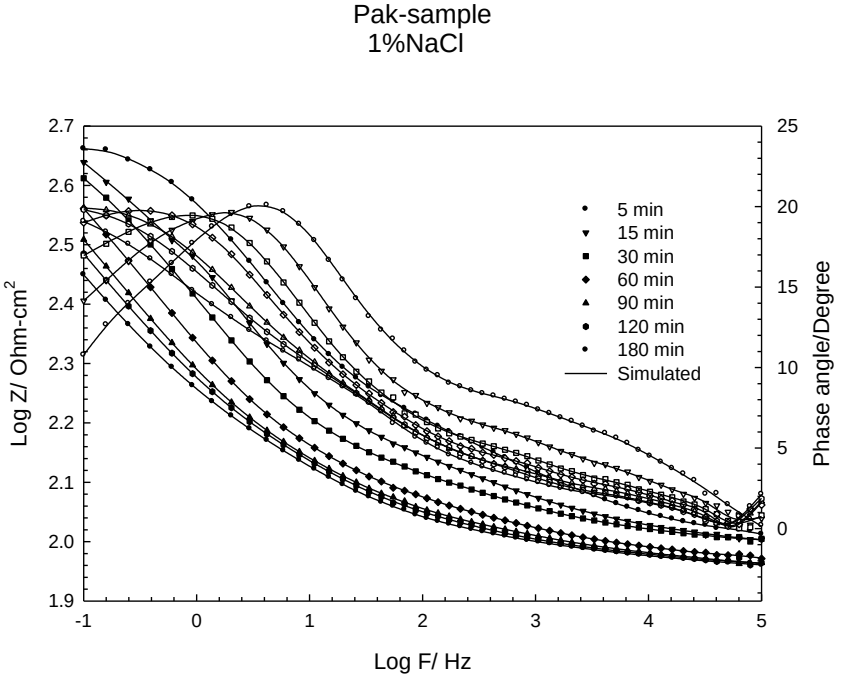

Figure 7. a Bode plots for a service sample (Pakistan) in 1% NaCl solution.

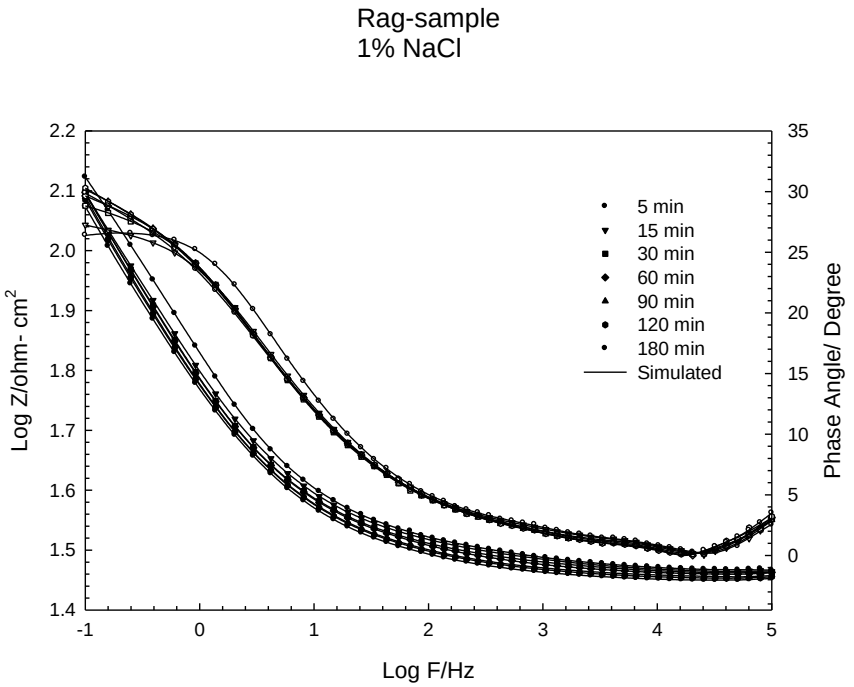

Figure 7. b Bode plots for a service sample (Ragusa) in 1% NaCl solution.

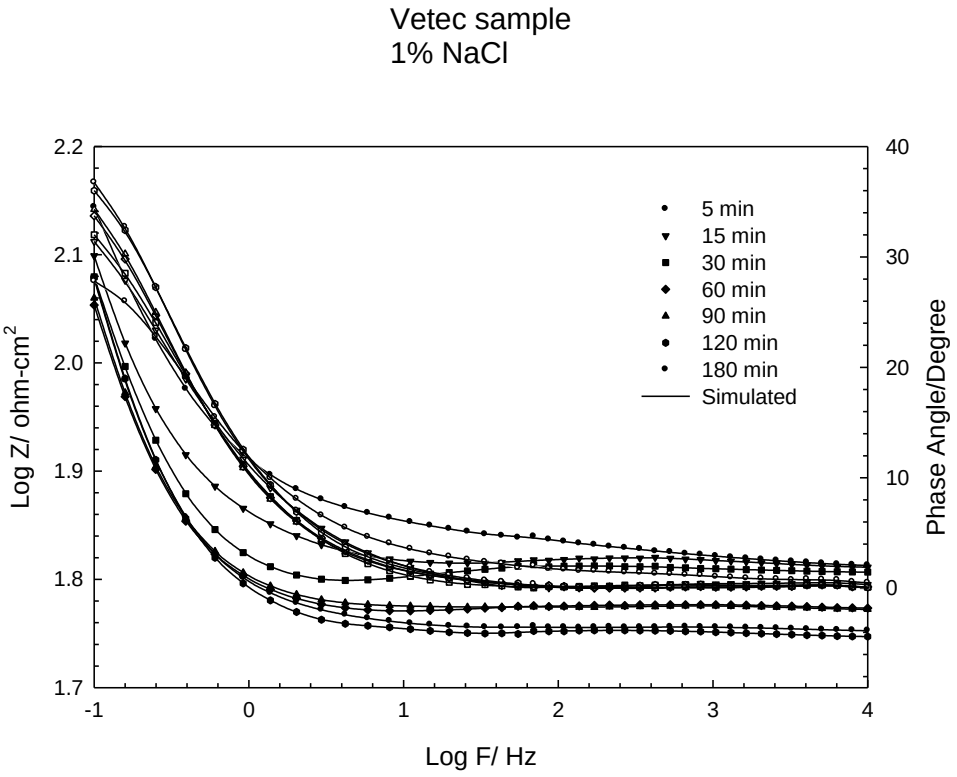

Figure 8. a Bode plots for Lab-sample [VETEC X65 Sample (1)] in 1% NaCl solution.

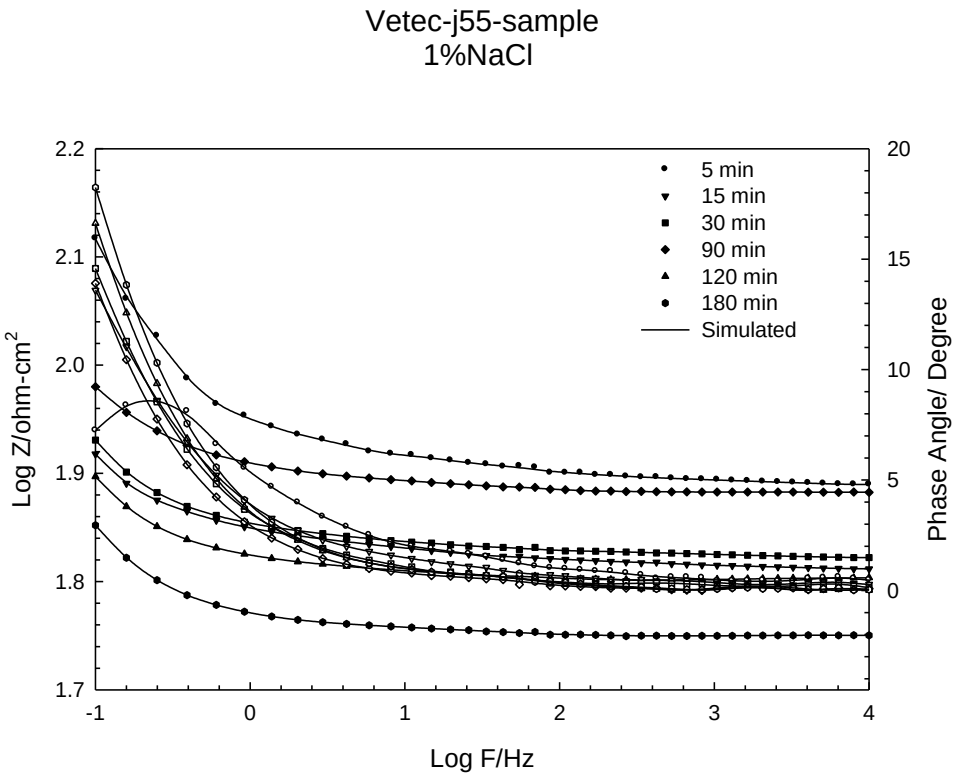

Figure 8. b Bode plots for Lab-sample [VETEC J55 Sample (1)] in 1% NaCl solution**.**

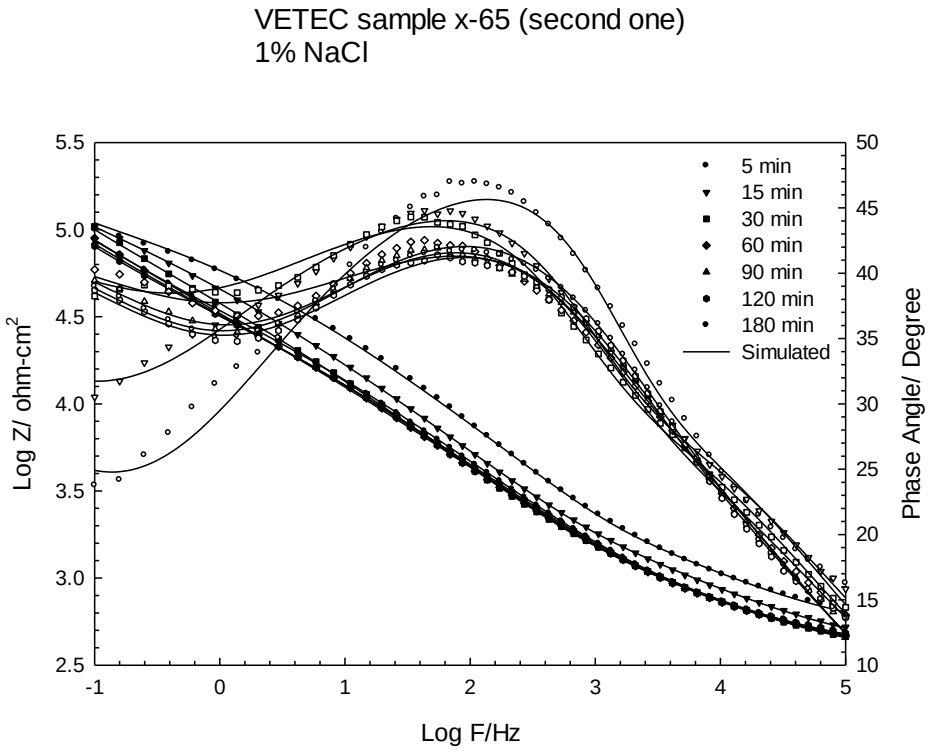

Figure 9. a Bode plots for Lab-sample [VETEC X65 Sample (2)] in 1% NaCl solution**.**

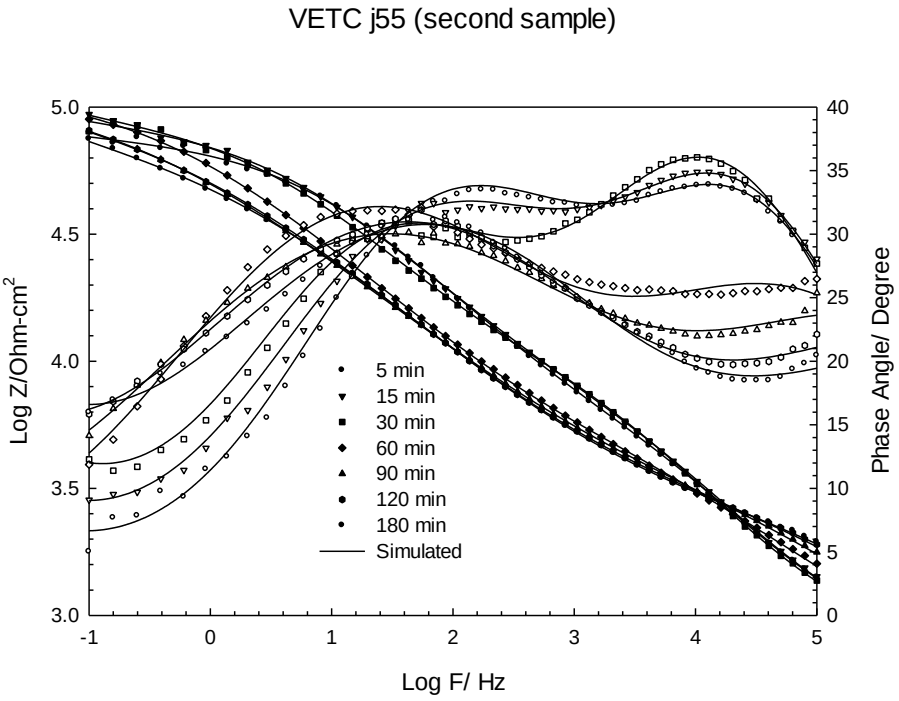

Figure 9. b Bode plots for Lab-sample [VETEC J55 Sample (2)] in 1% NaCl solution.

The impedance figures for all the samples as a function of immersion time (5-180 min.) were shown in Figs. 7-9. A capacitive behavior was observed at a high frequency range, which could be attributed to a double layer between the corrosion scale and the electrode surface. At low frequency, a characteristic diffusion process was assigned clearly, and expected to be finite-thickness boundary layer diffusion. It is known that at a high and middle frequency, finite-thickness boundary layer diffusion impedance is as same as Warburg impedance (semi-infinite boundary diffusion impedance) [23]. Actually, the corrosion rate is controlled mainly by ions diffusion rate in the corrosion scale, when the steel surface is covered with corrosion products [23]. Palacios and Shadley [24] showed that the adhesion and the thickness of the iron carbonate scale on the steel surface depend mainly on the microstructure of specimen. They concluded that the scales formed on normalized samples (N80 and 1018) were thicker and more adherent than those formed on the N80 Q&T ones. For all the measured samples (Figs. 7-9), a characteristic resistive region at a high and low frequency, and a capacitive behavior at intermediate frequency, with very small phase angle, and no plateau at low frequency were recorded. This emphasized the diffusion phenomena at the electrode-solution interface. The impedance data were analyzed using software provided with the electrochemical workstation IM6e Zahner-Elektrik. For a simple Randles equivalent circuit model consisting of a parallel combination of a capacitance, C_{dl}, and a resistor, R_p, in series with a resistor, R_s, representing the solution resistance, the electrode impedance, Z, is represented by the equation:

$$Z= R_s + R_p/ 1+ (2\pi f R_p C_{dl})^{\alpha} \quad (7)$$

Where α is an empirical parameter ($0 \leq \alpha \leq 1$) and (f) is the frequency in Hz. The above relation considers the deviation from the ideal capacitor (R-C) behavior in terms of a distribution of time constants due to variations in compositions or properties of the surface film. The best fitting of the data was obtained using the equivalent circuit model shown in Fig. 10.

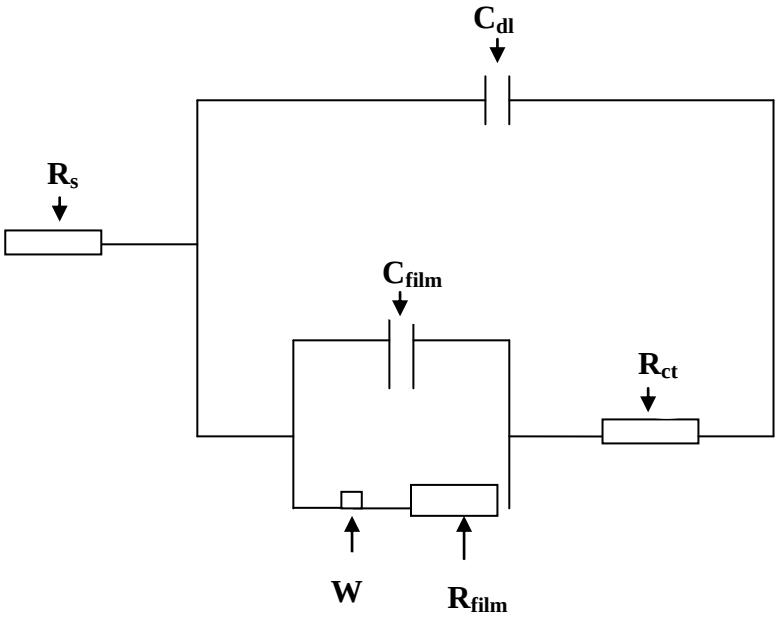

Figure 10. Equivalent circuit model.

In this equivalent circuit, the R_{film}-C_{film} combination was added to stand for the scales (carbonate) film. The experimental data and the proposed model were in a good match. This model comprised of a resistor, R_s, representing the solution resistance in series to two parallel combinations, R_{ct} and C_{dl} representing the charge transfer resistance and the double layer capacitance. R_{film}-C_{film} and Warburg impedance (W) were introduced to the cell to assign the carbonate (corrosion products) film resistance, capacitance, and diffusion process respectively. The diffusion process may indicate that the corrosion mechanism is controlled not only by a charge transfer process but also by diffusion transfer as well. The values of the equivalent circuit parameters were computed and introduced in Tables (4-9).

Table 4. Electrochemical impedance parameters for a service sample (Pakistan) in 1% NaCl solution.

Time (min.)	R_s (Ω)	C_{dl} uFcm^{-2}	R_{ct} (Ωcm^2)	C_{film} uFcm^{-2}	R_{film} (Ωcm^2)	α_{dl}	α_{film}	W (kΩ s$^{-1/2}$)
5	6.3	1.35	176	12.1	690.0	0.90	0.73	8.2
15	8.6	3.08	144	27.3	345.6	0.90	0.80	138.2
30	9.1	3.8	97.4	32.7	373.4	0.60	0.76	193.7
60	8.6	4.4	87.9	37.5	390.7	0.60	0.71	127.1
90	9.1	8.2	58.6	12.8	312.5	0.60	0.65	116.3
120	9.3	12.1	143.0	3.2	296.6	0.62	0.65	9.01
180	9.3	13.3	85.4	2.3	277.0	0.62	0.65	11.44

Table 5. Electrochemical impedance parameters for a service sample (Ragusa) 1% NaCl solution.

Time (min.)	R_s (Ω)	C_{dl} uFcm^{-2}	R_{ct} (Ωcm^2)	C_{film} uFcm^{-2}	R_{film} (Ωcm^2)	α_{dl}	α_{film}	W (kΩ s$^{-1/2}$)
5	8.3	38.6	10.7	216.2	14.4	0.55	0.84	16.7
15	8.1	48.1	12.6	183.7	16.1	0.60	0.82	11.8
30	8.1	50.8	11.5	195.4	19.3	0.65	0.80	11.9
60	8.1	58.3	10.6	150.5	30.8	0.67	0.77	12.0
90	7.9	62.3	9.1	144.8	34.5	0.68	0.77	12.9
120	7.9	63.9	9.1	136.8	38.0	0.68	0.77	12.2
180	7.9	66.1	9.5	39.4	116.9	0.68	0.75	7.5

Table 6. Electrochemical impedance parameters for VETEC X65 Sample (1) in 1% NaCl solution.

Time (min.)	R_s (Ω)	C_{dl} uFcm^{-2}	R_{ct} (Ωcm^2)	C_{film} uFcm^{-2}	R_{film} (Ωcm^2)	α_{dl}	α_{film}	W (kΩ s$^{-1/2}$)
5	9.2	31.2	5.1	362.3	8.0	0.55	0.76	1.1
15	9.2	32.0	0.80	942.0	16.6	0.62	0.82	1.3
30	9.1	36.6	0.44	1536	25.87	0.66	0.85	1.5
60	8.4	37.5	0.38	1630	43.67	0.67	0.87	1.57
90	8.4	37.5	0.30	1653	55.14	0.67	0.87	1.59
120	8.1	36.8	0.36	1601	60.05	0.67	0.88	1.56
180	8.1	36.7	0.37	1597	66.05	0.67	0.88	1.56

Table 7. Electrochemical impedance parameters for VETEC J55 Sample (1) 1% NaCl solution

Time (min.)	R_s (Ω)	C_{dl} uFcm^{-2}	R_{ct} (Ωcm^2)	C_{film} uFcm^{-2}	R_{film} (Ωcm^2)	α_{dl}	α_{film}	W (kΩ s$^{-1/2}$)
5	16.2	22.5	11.8	456.5	5.38	0.50	0.71	2.79
15	13.3	11.8	5.7	1652	6.01	0.55	0.62	2.57
30	13.7	8.2	4.6	1978	7.03	0.55	0.63	2.77
60	15.8	5.8	4.3	2130	9.02	0.60	0.64	2.90
90	13.2	1.9	2.8	3065	25.01	0.65	0.70	3.90
120	11.7	1.25	2.4	3804	47.01	0.67	0.80	4.90
180	13.5	1.20	2.8	3739	50.01	0.67	0.80	4.90

Table 8. Electrochemical impedance parameters for VETEC X65 Sample (2) in 1% NaCl solution.

Time (min.)	R_s (Ω)	C_{dl} uFcm^{-2}	R_{ct} (kΩcm^2)	C_{film} uFcm^{-2}	R_{film} (kΩcm^2)	α_{dl}	α_{film}	W (kΩ s$^{-1/2}$)
5	60.5	0.059	3.70	0.025	107.0	0.63	0.86	5.8
15	46.8	0.078	3.73	0.038	142.5	0.61	0.79	9.1

30	43.1	0.097	3.55	0.046	110.3	0.61	0.78	20.3
60	43.4	0.10	3.14	0.032	73.5	0.60	0.79	19.7
90	47.2	0.097	2.60	0.036	42.7	0.66	0.69	12.1
120	47.4	0.095	2.10	0.032	44.2	0.65	0.70	11.3
180	48.1	0.093	2.10	0.032	45.7	0.66	0.70	11.9

Table 9. Electrochemical impedance parameters for VETEC J55 Sample (2) in 1% NaCl solution.

Time (min.)	**R_s (Ω)**	**C_{dl} uFcm^{-2}**	**R_{ct} (kΩcm^2)**	**R_{film} (kΩcm^2)**	**α_{dl}**	**α_{film}**	**W (kΩ s$^{-1/2}$)**
5	85.5	0.01	7.6	66.7	0.66	0.60	0.72
15	86.0	0.01	8.6	78.5	0.66	0.59	1.1
30	86.0	0.011	11.2	77.8	0.67	0.59	1.9
60	67.7	0.013	6.3	111.0	0.64	0.62	0.36
90	43.7	0.011	4.3	110.0	0.63	0.61	0.45
120	33.5	0.01	3.8	96.7	0.62	0.60	1.6
180	32.0	0.01	3.6	81.0	0.60	0.59	2.0

It was observed from the tables that: in both Pakistan and Ragusa service samples, the film resistance R_{film} increased with the immersion time, whereas the film capacitance C_{film} decreased. And for both VETEC samples (sample 1), the R_{film} decreased with immersion time and the capacitance (which is inversely proportional to the film thickness) increased. This means that Ragusa and Pakistan service samples have a more resistive film (corrosion products film) than that formed on VETEC (samples 1) specimens. Whereas the second prepared Two VETEC (samples 2) specimens showed a higher R_{film} value and almost a constant film thickness with immersion time. The lower estimation of α (0.6) assigned the presence of a diffusion process at the interface [16].

The presence of different anions like Cl^-, Br^- or I^- can promote the iron dissolution in aqueous solutions [25, 26]. Ueda and Takabe [27] studied the characteristics of two steels of different composition and heat treatments in 5% NaCl solution. They concluded that lamellar cementite enhances the dissolution of iron, as it acts as a cathodic site. Thus, leads to the increase of the local concentration of Fe^{2+} ions in the cavities between cementite platelets, Lamellar cementite, which anchors the corrosion product.

To consider the interaction of chloride ions, the following equations have been proposed:

$$Fe + Cl^- \rightarrow FeCl^-_{ads} \quad (8)$$

$$FeCl^-_{ads} \rightarrow FeCl^+ + 2e^- \quad (9)$$

$$FeCl^+ \rightarrow Fe^{2+} + Cl^- \quad (10)$$

The adsorbed species $FeCl^-$ is worthy of special interest in the corrosion mechanism since it could induce the formation of iron oxides with a porous characters, and the localized corrosion of the

steel; improving the diffusion of aggressive species. The diffusion process might be accompanied by the iron ions formed at the metal-film interface and a precipitation of different iron compounds on the steel surface.

For the LPR measurements (figures not shown), it was found that the calculated polarization resistance (R_p) after 180 min of the sample immersion in 1% NaCl has almost the same trend like that got from the EIS measurements after the same immersion time, as can be seen in Table (10).

Table 10. The polarization resistance from (EIS) and (LPR) measurements after 180 min. from the sample immersion in 1% NaCl

Sample	**R_p (LPR)$_{180\ min}$ (Ohm cm^2)**	**R_p (EIS)$_{180\ min}$ (Ohm cm^2)**
Service sample (Pakistan)	430.1	277
Service sample (Ragusa)	196.7	116.9
VETEC j55 (sample 1)	192.3	66.01
VETEC x65 (sample 1)	152.7	50.05
VETEC x65(sample 2)	16.2 k ohm	45.5 k ohm
VETEC j55(sample 2)	22.7 k ohm	81.0 k ohm

It was found from EIS and LPR data, that the second prepared VETEC samples (VETEC sample 2) have a considerable higher corrosion resistance and a better performance than the first prepared VETEC samples, which could be more comparable to the field service samples (Pakistan and Ragusa).

4. CONCLUSIONS

-Two types of specimens were provided, having surface layers grown during a service, or prepared under controlled conditions in the laboratory.

-The impedance measurements showed that Ragusa and Pakistan service samples have more resistive films (corrosion products films formed in the field) than those formed on VETEC lab-samples (films formed during the laboratory tests), whereas the second group of prepared samples showed a higher R_{film} value and almost a constant film thickness with immersion time.

-Electrochemical measurements results were compared by the film characterization performed with the optical techniques.

-Two layers of scales were observed in the samples exposed to different environments producing Carbonate film. The outer layer was formed by a dense conglomerate of large Iron Carbonate crystals but they did not give rise to a true polycrystal, while the inner layer corresponded to

the growth of the film inside the original metal surface. Such inner layer contained a dispersed Iron Carbide phase deriving directly from the Perlite phase in the steel substrate. Another phase (Cementite) was observed. Its phase remained not altered by corrosion phenomena

- For the LPR measurements, it was found that the calculated R_p values (after 180 min of the sample immersion in 1% NaCl) have a similar trend to that recorded from the EIS measurements after the same time.

-The methods to grow surface films developed in the frame of the present work seemed to offer the opportunity to grow reproducible and representative layers on the steel pipeline.

-Producing simulated scales layers successfully in the Lab., enables us to put a predictive model for the scales formation and characterizations.

References

1. R. Grimm, D. Landolt, *Corrosion Science*, 36 (1994) 1847.
2. G. Gabetta, A. Bennardo, S. Diliberto, "Discussion of laboratory tests results with the aid of computational fluid dynamics", paper 03347, *Corrosion J. San Diego*, (2003).
3. A. Bennardo, G. Gabetta, "Evaluation of erosion/corrosion on a pipe bend due to fluid dynamic. Comparison between numerical simulations and the real case", paper n°144, 11th International Conference on Multiphase Flow in industrial plants, Palermo, 7-10 Sept. (2008).
4. M. JOHNSON, M. TOMSON, Corrosion/91 Paper 268, NACE International, Houston, Texas, (1991)
5. W. SUN, S. NEŠIĆ, Corrosion/06, Paper 365, NACE International, Houston, Texas, (2006).
6. G. Gabetta, V. Balostro, G. Bolzon, M. Battagliarin, B. Molinas, "MECHANICAL PROPERTIES OF IRON-BASED SCALES IN CO2 CORROSION MODELING", Workshop "Research in Progress, Corrosion Modelling", Nace Corrosion, Salt Lake City, (2012).
7. L. Yan, L. Niu, H. Lin, W. Wu, S. Liu, *Corros. Sci*., 41 (1999) 2305.
8. Z. Yin, W. Zhao, Z. Bai, Y. Feng, W. Zhou, *Electrochim. Acta, 53* (2008) 3690.
9. J. Sardisco, W. Wright, E. Greco, *Corrosion*, 19 (1963) 353.
10. D. Shoesmith, P. Taylor, M. Bailey, D. Owen, *J. Electrochem. Sci. Technol*., 127 (1980) 1007.
11. H. Vedage, T. Ramanarayanan, J. Munford, S. Smith, *Corrosion*, 49 (1993) 114.
12. H. Castaneda, E. Sosa, M. Espinosa-Medina, *Corros. Sci*., 51 (2009) 799.
13. E. Sosa, R. Cabrera-Sierra, I. Garca, M. Oropeza, I. Gonzlez, *Corros. Sci.*, 44 (2002) 1515.
14. R. Cabrera-Sierra, E. Sosa, M. Oropeza, I. Gonzlez, *Electrochim. Acta*, 47 (2002) 214.
15. S. Nesic, K. Lee, Electrochim. Acta, 47 (2002) 2149.
16. R. El-Sherif, K. Ismail, W. Badawy, *Electrochim. Acta*, 49 (2004) 5139.
17. W. Badawy, R. El-Sherif, H. Shehata, *Electrochimica Acta*, 54 (2009) 4501-4505.
18. R. Reed-Hill, Physical Metallurgy Principles, 2nd ed., Litton Educational Publishing International, Mexico, (1979).
19. C. de Waard, D. Milliams, *Corrosion*, 31(1975) 177- 181.
20. E. Dayalan, G. Vani, J. Shadley, S. Shirazi, E. Rybicki, *Corrosion*/ 95, NACE International, 1995, paper No. 118.
21. R. Hausler, D. Stegmann, *Corrosion*/88, NACE, 1988, paper No. 863.
22. A. Dugstad, *Corrosion*/92, Houston, TX, NACE, 1992, paper No. 14.
23. B. Kinsella, Y. Tan, S. Balley, *Corrosion*, 54 (10) (1998) 835.
24. C. Palacios, J. Shadley, *Corrosion*, 47 (1991) 122.
25. J. Banas, U. Lelek-Borkowska, B. Mazurkiewicz, W. Solarski, *Electrochim. Acta, 52* (2007) 570.

26. T. Kawai, H. Nishihara, K. Aramaki, *Corros. Sci.*, 38 (1996) 225.
27. M. Ueda, H. Takabe, in: Proceedings of NACE Corrosion/99 (NACE 1999), San Antonio, TX, 1999, Paper No. 13.